



HAL
open science

Calibrated work function mapping by Kelvin probe force microscopy

Pablo Fernández Garrillo, Benjamin Grevin, Nicolas Chevalier, Lukasz Borowik

► To cite this version:

Pablo Fernández Garrillo, Benjamin Grevin, Nicolas Chevalier, Lukasz Borowik. Calibrated work function mapping by Kelvin probe force microscopy. *Review of Scientific Instruments*, 2018, 89 (4), pp.043702. 10.1063/1.5007619 . hal-02277068

HAL Id: hal-02277068

<https://hal.science/hal-02277068v1>

Submitted on 2 Jun 2022

HAL is a multi-disciplinary open access archive for the deposit and dissemination of scientific research documents, whether they are published or not. The documents may come from teaching and research institutions in France or abroad, or from public or private research centers.

L'archive ouverte pluridisciplinaire **HAL**, est destinée au dépôt et à la diffusion de documents scientifiques de niveau recherche, publiés ou non, émanant des établissements d'enseignement et de recherche français ou étrangers, des laboratoires publics ou privés.

Calibrated work function mapping by Kelvin probe force microscopy ^{EP}

Cite as: Rev. Sci. Instrum. **89**, 043702 (2018); <https://doi.org/10.1063/1.5007619>

Submitted: 02 October 2017 • Accepted: 12 March 2018 • Published Online: 03 April 2018

 Pablo A. Fernández Garrillo, Benjamin Grévin, Nicolas Chevalier, et al.

COLLECTIONS

 This paper was selected as an Editor's Pick



View Online



Export Citation



CrossMark

ARTICLES YOU MAY BE INTERESTED IN

[Kelvin probe force microscopy](#)



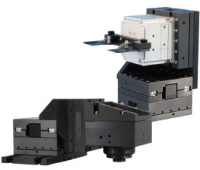
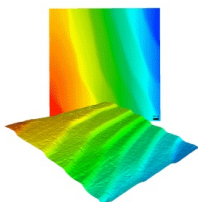
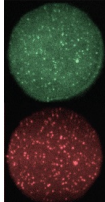
Applied Physics Letters **58**, 2921 (1991); <https://doi.org/10.1063/1.105227>

[High-sensitivity quantitative Kelvin probe microscopy by noncontact ultra-high-vacuum atomic force microscopy](#)

Applied Physics Letters **75**, 286 (1999); <https://doi.org/10.1063/1.124357>

[Practical aspects of single-pass scan Kelvin probe force microscopy](#)

Review of Scientific Instruments **83**, 113701 (2012); <https://doi.org/10.1063/1.4761922>

 MCL MAD CITY LABS INC. www.madcitylabs.com	<p>Nanopositioning Systems</p> 	<p>Modular Motion Control</p> 	<p>AFM and NSOM Instruments</p> 	<p>Single Molecule Microscopes</p> 
---	--	--	---	--

Calibrated work function mapping by Kelvin probe force microscopy

Pablo A. Fernández Garrillo,¹ Benjamin Grévin,² Nicolas Chevalier,¹
and Łukasz Borowik^{1,a)}

¹Univ. Grenoble Alpes, CEA, LETI, 38000 Grenoble, France

²Univ. Grenoble Alpes, CNRS, CEA, INAC, SYMNES, 38000 Grenoble, France

(Received 2 October 2017; accepted 12 March 2018; published online 3 April 2018)

We propose and demonstrate the implementation of an alternative work function tip calibration procedure for Kelvin probe force microscopy under ultrahigh vacuum, using monocrystalline metallic materials with known crystallographic orientation as reference samples, instead of the often used highly oriented pyrolytic graphite calibration sample. The implementation of this protocol allows the acquisition of absolute and reproducible work function values, with an improved uncertainty with respect to unprepared highly oriented pyrolytic graphite-based protocols. The developed protocol allows the local investigation of absolute work function values over nanostructured samples and can be implemented in electronic structures and devices characterization as demonstrated over a nanostructured semiconductor sample presenting $\text{Al}_{0.7}\text{Ga}_{0.3}\text{As}$ and GaAs layers with variable thickness. Additionally, using our protocol we find that the work function of annealed highly oriented pyrolytic graphite is equal to 4.6 ± 0.03 eV. *Published by AIP Publishing.* <https://doi.org/10.1063/1.5007619>

INTRODUCTION

To a large extent, the work function (WF) is the minimum energy needed to remove an electron to a point in the vacuum immediately outside of the surface and it is defined by the difference between the Fermi level E_f and the vacuum level E_{vacuum} as defined by Cahen and Kahn.¹ The WF is a parameter of utmost importance in the description and control of any electronic device behavior as well as charge carrier injection and transport. Moreover, due to its sensitivity to chemical variations on surfaces, its measurement can be used as a tool to investigate surface conditions.² The WF has also significant importance in the fields of electroluminescence and photovoltaics, for instance, it influences the band line-up at the interface between organic materials and electrodes, which is also noteworthy in the development of organic light-emitting diodes.³

Furthermore, the WF is an important parameter for the characteristics of electric arcs, particularly for the electronic emission in the case of contact materials.⁴

There exist several methods used to measure the WF of a material. Among those methods, one can find techniques based on thermionic emission, methods based on photoemission, and the Kelvin probe method as proposed in the 19th century by Lord Kelvin, to name a few.^{5–7} However, the majority of these approaches lack the spatial resolution required for the characterization of electronics components, not to mention nano-objects or nanostructured surfaces (i.e., nanowires, nanocrystals, and III-V nano-hetero-structures).

An exception to this is Kelvin probe force microscopy (KPFM) proposed by Nonnenmacher *et al.*,⁸ which provides spatially resolved measurements of the surface potential of conducting and semi-conducting samples. In principle,

this surface potential, also called contact potential difference (CPD), provides the WF difference between the surface under investigation and the probe (i.e., a relative value of the surface's WF). Nevertheless, this method can be used to acquire an absolute WF value if the probe's WF value is known.⁹

The probe's WF can be found by calibrating the probe against a reference surface with known WF. Highly oriented pyrolytic graphite (HOPG) is often used as this reference for several reasons such as availability, cost, low resistivity, and its hydrophobic properties among others. However, HOPG WF values found in the literature are very much dispersed, ranging from a value below 4.5 eV^{10–12} to as high as 5 eV,^{9,13–15} and such dispersion of WF values can potentially introduce a high uncertainty level in the probe's WF calibration, which in turn compromises the WF measure obtained over the surface of interest. We note that large dispersion of HOPG WF values in the literature can be found even for measurements under the same environmental conditions: under air from 4.6 eV to 5 eV^{9,14,16,17} and in ultra-high vacuum (UHV) from 4.48 eV to 5 eV.^{10,13,17–19} Theory predicts a value between 4.46 eV and 4.64 eV depending on the number of layers.²⁰ Thus, attention must be paid when choosing the HOPG reference value. Furthermore, HOPG WF values can be quite laterally dispersed over a measured surface (up to few hundreds mV), even if measurements are acquired over micrometer areas.^{21–23} However, it must also be noted that such strong WF variation on HOPG can be due to the presence of surface contamination.²⁴ Thus, samples with such WF dispersion should be avoided as references for KPFM tip calibration.

To illustrate the lateral WF variation on a clean HOPG sample, we performed measurements presented on Fig. 1. In this experiment, we measured both topography and CPD of a mechanically under air delaminated ZYB grade HOPG sample, provided by the Bruker Company. The sample was

^{a)}Author to whom correspondence should be addressed: lukasz.borowik@cea.fr

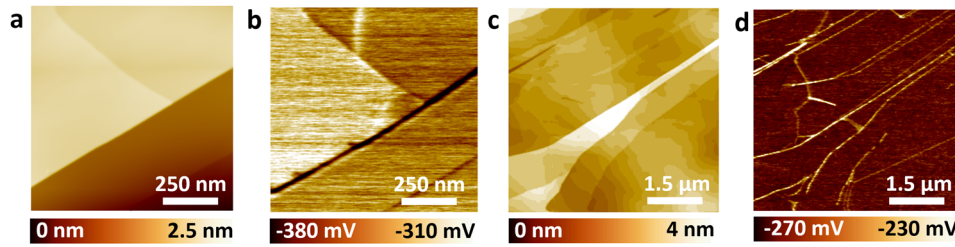


FIG. 1. Topography [(a) and (c)] and CPD [(b) and (d)] images on HOPG by FM-KPFM. AFM detuning frequency was $\Delta f = -25$ Hz. FM-KPFM was implemented using a modulation frequency $f = 958$ Hz and electrostatically excited with $V_{ac} = 500$ mV. Sample presented on images: (a) and (b) are as-cleaved (without annealing), (c) and (d) were annealed in UHV to 700 °C during 30 min.

exposed very shortly to ambient conditions. Measurements were acquired under UHV conditions by atomic force microscopy (AFM) combined with single-pass frequency modulation (FM)-KPFM.²⁵ Here we use a Nanosensors PtIr-PPP-EFM probe with a resonance frequency of ca. 61.2 kHz. The three-dimensional distribution of chemical composition on this kind of tip was measured.²⁶ Additionally to the measurements on the as-cleaved sample [Figs. 1(a) and 1(b)], UHV annealing was performed on the same sample for different temperatures: 300 °C, 600 °C, and 700 °C [Figs. 1(c) and 1(d)], each time during 30 min. The annealing performed at temperatures lower than 700 °C did not provide a smoothing of the sample's surface potential; even after the annealing cycles at 300 °C and 600 °C, the surface potential images (not shown here) displayed multiple dark and white patches and a CPD contrast as high as 60 mV. By contrast, the CPD of the 700 °C annealed sample is uniform (with the exception of flakes' edges) and it reveals a homogeneous CPD = -260 ± 15 mV on the HOPG flakes. This experiment proves that in the case of HOPG, a sample preparation is needed to obtain consistent WF values. Nevertheless, the different values of HOPG WF found in the literature can lead to confusion. To dispel these doubts, in a further part of this work, the HOPG WF value will be calculated using the proposed calibration protocol presented in this article.

As mentioned before, the WF is a parameter extremely sensitive to chemical variations, and surface state (i.e., contaminants, oxide)^{2,27} consequently measurements reproducibility stands as a challenge. In view of this, it becomes evident that in order to perform trustworthy absolute WF measurements, surface modification during measurement shall be avoided.

In this paper, we propose and demonstrate a protocol to acquire precise absolute WF measurements using different monocrystalline metallic reference samples with known surface orientation as an alternative to HOPG. In that endeavor, we use non-contact (nc)-AFM combined with single-pass FM-KPFM under ultra-high vacuum (UHV) conditions.²⁵ This configuration offers several advantages, for instance, the use of nc-AFM prevents any physical contact between the probe and the sample, in contrast to intermittent contact mode, where the sample's surface can be modified by the probe upon physical contact and vice versa.²⁸ This configuration also allows us to maintain a constant effective distance between the probe and the sample. Furthermore, the use of single-pass KPFM prevents drift artefacts and offers an increased

sensitivity as well as an improved lateral resolution compared to double-pass KPFM.²⁹ Additionally, under UHV, both probe and samples can be stored after preparation without suffering any substantial surface modification for a time period ranging from several days to few weeks depending on sample composition.

Here, different metallic reference surfaces with known crystalline orientation (hence, known WF) are used for the WF calibration of an AFM probe. The calibrated probe is then used to map the local variation of the absolute WF over a nanostructured sample. With this approach, absolute and reproducible WF values were acquired with an improved uncertainty with respect to HOPG-based protocols.

METHODS

Here, three monocrystalline metallic samples with known crystallographic orientation, Ag(111), Cu(100), and Al(110) are proposed as reference surfaces for probe's WF calibration. All reference samples, which are commercially available, were provided by the Goodfellow Cambridge Limited Company and stoked in UHV conditions during measurements. Prior to this, all samples were stocked in ambient conditions. While the proposed samples are not equally adapted for WF calibration (i.e., different oxidation rates, surface roughness, surface contamination, cost, etc.), the purpose of having three different metallic samples is to verify the self-consistency of results. Additionally, the above mentioned samples were selected following the criteria of having the maximum possible gap between their known WF values (see Table I).

Note that values presented in Table I can largely vary from one author to the other, for Ag(111),^{33–40} Cu(100),^{41–47} and Al(110).^{48,49} The publications which group WF values for various materials^{50–53} can often be useful. WF values for proposed samples were selected upon critical examination of methods including the use of an ultrahigh vacuum system and reduced uncertainty values (this last parameter was not always available).

TABLE I. WF values found in the literature for proposed samples.

	Ag(111) (eV) ³⁰	Cu(100) (eV) ³¹	Al(110) (eV) ³²
ϕ_{Sample}	4.74 ± 0.02	4.59	4.06 ± 0.03

In the used setup, the compensation bias is applied to the probe, and consequently, the probe's WF can be determined as KPFM yields a CPD that can be expressed as

$$V_{Probe} = CPD = \frac{\phi_{Probe} - \phi_{Sample}}{|e|}. \quad (1)$$

Here, V_{Probe} represents the compensation bias, ϕ_{Probe} represents the probe's WF, ϕ_{Sample} represents the sample's theoretical WF, and e represents the elementary charge.

Following a surface cleaning procedure which shall include both the samples and the probe (to ensure clean surfaces free of contaminants that could modify the expected WF value), the probe is calibrated against each one of the samples separately. In this step, it is assumed that each sample's WF corresponds to a known value^{30–32,54} and that the probe's WF is constant over time.

Which such an approach and if samples are correctly prepared, the probe's absolute WF calibration over each sample should yield approximately the same result.

To illustrate this, a Nanosensors PtIr–PPP-EFM probe with a resonance frequency of ca. 65.7 kHz previously *in situ* heated at 150 °C for 20 min was used to obtain CPD measurements over each sample. This heating step is of crucial importance to ensure the probe's WF stability over time. Indeed, by heating the probe we removed the adsorbed water from the probe's surface which can induce strong variations on the probe's WF value over time. WF calibrations performed on unprepared probes proved that this adsorbed water can modify the measured probe's WF value. We noticed that for some cases of air exposed and non-prepared probes WF value can change as much as 600 meV over a 24-h time period due to water layer modification on the tip cone. In all cases, tip stability should be observed during the calibration process to avoid tip changes.⁵⁵ This can be done by verification of CPD sameness during the experiment using one of the calibrations samples.

During these measurements, topography and CPD were simultaneously acquired by FM-KPFM and nc-AFM. In all cases, AFM detuning frequency was $\Delta f = -10$ Hz. FM-KPFM was implemented using a modulation frequency $f = 1$ kHz and electrostatically excited with $V_{ac} = 500$ mV. As discussed previously⁵⁶ in some cases CPD can vary in the function of tip-surface distance. In our case (metalized tip and homogeneous metal sample surfaces), we did not notice the distance-dependent CPD values when changing the detuning frequencies of -25 Hz to -5 Hz. However, as a matter of coherence we kept the same detuning frequency for all calibration samples.

Prior to the probe's calibration, as previously mentioned, samples' surface preparation is needed. In general, surface cleaning means the removal of natural contaminants, i.e., O, C, and H containing species which form surface layers of only a few-nanometer thickness yet enough to modify a sample's WF. Therefore, a clean, homogeneous surface is of utmost importance when calibrating the KPFM probe's WF.

Surface sputtering by ion bombardment is a common choice for *in situ* surface cleaning. It offers many advantages, e.g., practicability and easy integration into UHV systems,

TABLE II. Sputtering and annealing cycles' duration over all samples.

		Al(110) (h)	Cu(100) (h)	Ag(111) (h)
First cycle		2/3.5	0.5/0.5	2/1
Second cycle	Sputtering/	2/2	1.5/>>6	1/>>6
Third cycle	annealing	5/2.5	4/4	3/>>6
Fourth cycle		2/2		

and it is a widely used standard procedure for surface cleaning.⁵⁷ Nonetheless, ion bombardment has some inherent side effects such as damage creation and particle implantation;⁵⁸ therefore, annealing of the bombarded surface will be necessary for surface reconstruction.

Here, samples were treated with low-energy sputtering to minimize damage creation and particle implantation⁵⁷ (500–600 eV Ar⁺ ions, current flux ≈ 40 $\mu\text{A}/\text{cm}^2$, and $P = 5 \times 10^{-5}$ mbar) and annealing cycles (temperatures ranging from 470 °C to 520 °C) following surface preparation procedures described elsewhere,^{59–61} until a ladder-like shape in the sub-nm scale consistent with atomic steps appears on the non-contact AFM topographic image acquired along with the WF immediately after each cycle. Sputtering and annealing cycles' duration over all samples are shown in Table II.

RESULTS AND DISCUSSION

Prior to surface treatment, samples displayed irregular surfaces, in some cases with topographic features of few hundreds of nanometers. After each surface treatment cycle, surfaces began to display more homogeneous surfaces. Topography images of the samples' surface at their final state (i.e., after surface preparation was completed) are shown in Fig. 2. In all cases Ag(111), Al(110), and Cu(100) samples, we see ladder-like shapes in the sub-nm scale consistent with atomic steps, indicating that a clean and reconstructed surface was attained. Additionally, the analysis of the damping images (not shown) recorded simultaneously with the KPFM data suggests a homogenous chemical nature at the surface of each of these samples. More precisely, a homogenous damping signal means that the dissipated energy of the probe's oscillation amplitude due to probe-surface interactions remains constant over the imaged area. Finally, acquired CPD images were also homogeneous, meaning that surface chemistry⁶² of the analyzed area is the regular.

Measured values of the CPD between the PtIr–PPP-EFM probe and all reference samples are given in Table III (see Fig. 3). These potential differences correspond to the mean value of several KPFM images acquired over the prepared samples and corroborated by several single-point measurements. The associated uncertainties correspond to the full width at half maximum value of the images' Gaussian distribution, as represented in Fig. 3. In all cases, CPD values were obtained in FM-KPFM using a modulation frequency of 1 kHz and electrostatically excited with $V_{ac} = 500$ mV. Concerning the stability of the tip work function, it must be noted that the final measurements of CPD's presented in Table III were completed after all samples' preparation steps

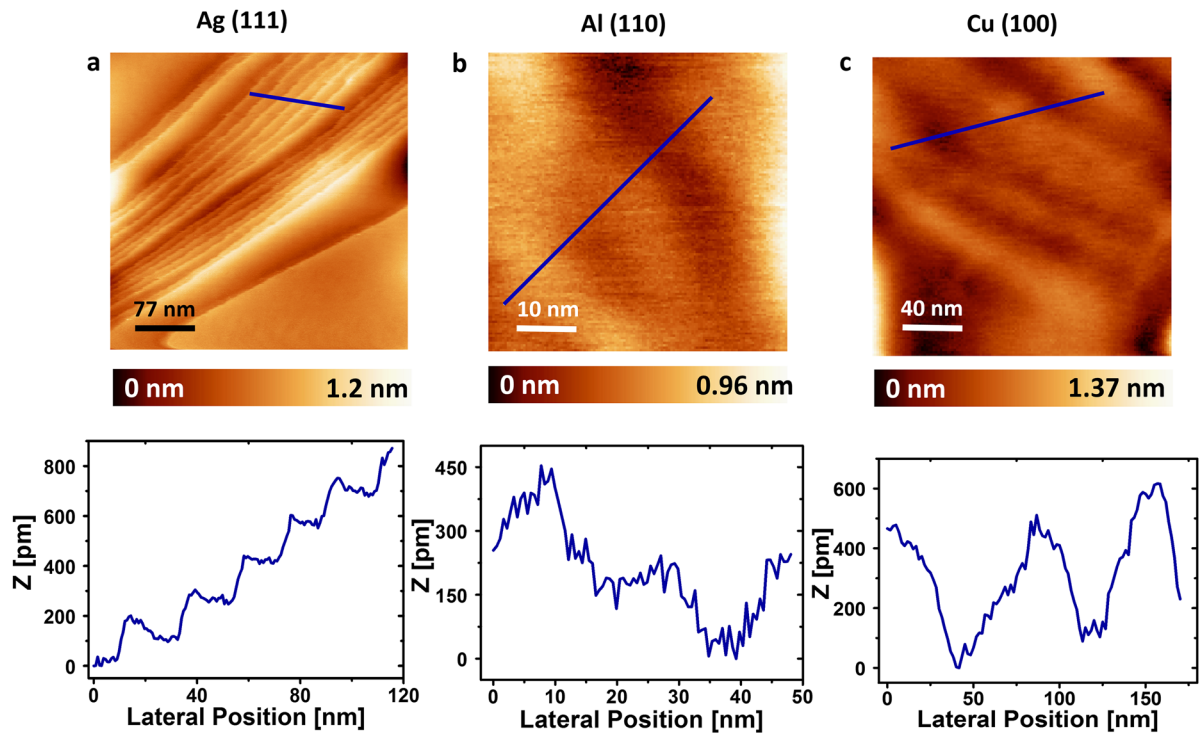


FIG. 2. Topography images and corresponding cross sectional profiles (blue line) of (a) Ag(111), (b) Al(110), and (c) Cu(100) samples after surface treatment, showing ladder-like shapes in the sub-nm scale. Images were acquired with a Pt coated Si probe. AFM detuning frequency was $\Delta f = -10$ Hz.

to avoid long time delay between CPD measurements. Additionally, at the end of calibration process we check the reproducibility of measurement with one of the calibration sample where we did not notice any change above uncertainty of CPD measurements.

Using Eq. (1) and assuming that each sample's WF correspond to values commonly found on the literature,^{30–32,54} we can obtain a probe's WF value for each sample. The difference between values establishes the measurement uncertainty. Results are shown in Table IV.

As shown in Table IV, probes' WF values found on different samples are comparable. It is then reasonable to assume a probe WF weighted value $\phi_{probe} = 4.82 \pm 0.03$ eV. Here, it is important to mention that the uncertainty values associated with the results of the calculation of the probe's WF using Cu(100) and Al(110) as references already include the original uncertainty values presented for these samples in Table I. On the other hand, the uncertainty of the probe's WF weighted value was obtained by comparing the results yielded by the calibrations against each one of the samples (see Table IV). Indeed, these results differed from each other by 60 meV at

the most (taking into account uncertainties), which allowed us to establish an uncertainty of ± 0.03 eV.

Using this probe with the known WF value, it has now become possible to directly measure the absolute WF value of samples under investigation with an improved energetic resolution compared to HOPG-based calibration methods and a lateral resolution that allows the investigation of nanostructured samples.

At this stage, this protocol can be applied to find the WF value on the previously measured ZYB grade HOPG sample. We will use here the sample annealed at 700 °C as it reveals a homogeneous CPD = -260 ± 15 mV on the HOPG flakes, the WF of the used probe is $\phi_{probe} = 4.34$ eV (Nanosensors PtIr-PPP-EFM probe with a resonance frequency of ca. 81.4 kHz). The calibrated HOPG WF value is equal to 4.6 ± 0.03 eV. This value agrees with the HOPG WF value theoretical value;²⁰ thus this measurement confirms that a value around 4.6 ± 0.03 eV should be used when a WF tip calibration with HOPG as the reference sample is performed.

Furthermore, we applied the above described protocol to map the WF over a sample of $Al_{0.7}Ga_{0.3}As$ and GaAs layers with variable thickness (BAM-L200 sample). A full description of the sample can be found elsewhere.⁶³

These measurements were made after a surface preparation which consisted in heating the sample under UHV conditions at 150 °C during 30 min in order to remove the adsorbed water from the sample's surface. Such preparation is essential to maximize the CPD contrast between materials as reported by Pouch *et al.*⁶⁴

TABLE III. Contact potential difference between probe tip and samples.

	Measured CPD (mV)
Cu(100)	252 ± 17
Al(110)	773 ± 16
Ag(111)	67 ± 18

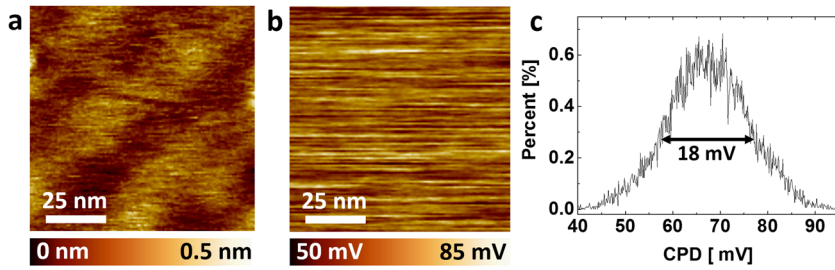


FIG. 3. (a) Topography and (b) CPD measurements on the Ag(111) sample. (c) CPD distribution measured from image (b) with full width at half maximum equal to 18 mV.

TABLE IV. Probe WF calculated from CPD measured on reference samples.

	Cu(100) (eV)	Al(110) (eV)	Ag(111) (eV)
ϕ_{Probe}	4.84 ± 0.017	4.83 ± 0.019	4.81 ± 0.02

Figure 4 depicts the BAM-L200 sample structure as well as the topography and CPD image acquired by nc-AFM combined with FM-KPFM using a previously calibrated Nanosensors PtIr-PPP-EFM probe with a WF value of 4.605 ± 0.03 eV and a resonance frequency of ca. 65.7 kHz previously heated at 150 °C for 20 min.

In this figure, we clearly see the CPD contrast between GaAs and $Al_{0.7}Ga_{0.3}As$ regions; this contrast agrees with previously reported studies.⁶⁴ WF measurements over GaAs and $Al_{0.7}Ga_{0.3}As$ regions give values of 4.45 ± 0.03 eV and 4.62 ± 0.03 eV, respectively.

In order to assess measured WF values, we compared them to theoretical WF values of GaAs and $Al_{0.7}Ga_{0.3}As$ as predicted by theoretical models.^{65,66} Given a sample silicon doping rate of $5 \times 10^{-7} \text{ cm}^{-3}$ (provided by the manufacturer and confirmed by a complementary ToF-SIMS analysis, not shown here), this model predicts a WF of 4.07 eV and 3.62 eV at room temperature for GaAs and $Al_{0.7}Ga_{0.3}As$, respectively. However, in our case, WF values measured over the sample, both in the case of GaAs and $Al_{0.7}Ga_{0.3}As$, are influenced by the presence of native oxides. For this reason, measured values are not expected to agree with theoretical ones. Indeed, the native oxide over the sample’s surface causes a positive band

bending of both GaAs and $Al_{0.7}Ga_{0.3}As$. In turn, results on GaAs are in good agreement with values previously obtained by other groups over a similar GaAs sample with oxide on its surface.^{67,68} Bastide *et al.* report a positive band bending of 400 meV in the case of GaAs due to the presence of oxide at the surface, consistent with our measurements, which explains the difference between theoretical and measured values.⁶⁷ Additionally, the WF contrast between GaAs and AlGaAs layers is also consistent with contrast values reported in a previous study.⁶⁴

Furthermore, we proceed to calibrate a Bruker super sharp silicon (SSS) probe with a resonance frequency of ca. 306.6 kHz, previously *in situ* prepared by Ar^+ sputtering with an energy of 5 keV during 30 min. Upon implementation of the above described protocol, the AFM probe revealed a WF value of 4.37 ± 0.03 eV. Thanks to its high aspect ratio this probe allowed the investigation of the local WF variation over the nanometer-thick layers present in sample’s zone 2 as depicted in Fig. 4. Additionally, the use of this probe serves to demonstrate that the calibration protocol can be implemented regardless of the AFM probe type.

Figure 5 shows the WF cross section acquired over the P₉-P₁₇ area, and we noticed that the WF contrast previously observed tends to decrease with the layers’ thickness and it disappears when the layers’ thickness drops below few nanometers. As it has been already demonstrated,⁶⁴ this decreasing tendency is due to an overlay of depletion layers, which causes a band bending overlap.

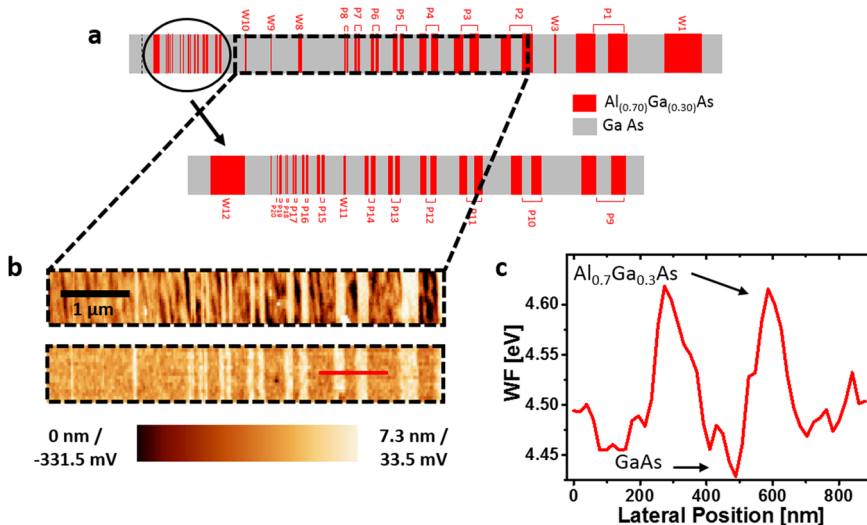


FIG. 4. (a) BAM-L200 strip pattern scheme. The doublet layers indexed from P₁ to P₈ and from P₉ to P₁₄ have been, respectively, certified by the fabricant from 587 to 76.5 nm and from 76.5 nm to 17.5 nm. Doublet layers indexed from P₁₅ to P₁₇ have been equally certified from 13.3 nm to 6.9 nm, respectively. The separated $Al_{0.7}Ga_{0.3}As$ layers indexed that W₈, W₁₀, and W₁₁ are certified to have a thickness of 38 nm, 14.2 nm, and 3.5 nm, respectively. (b) Topography and CPD measurements acquired over dashed-lined box area marked in (a). (c) CPD cross section acquired over P₃ doublet layers as shown in (b) by the red line.

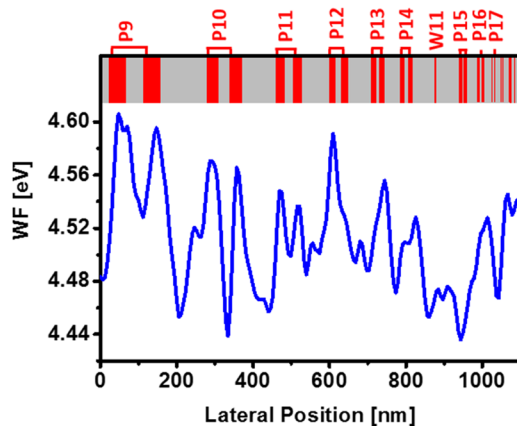


FIG. 5. WF cross section acquired by non-contact FM-KPFM using a SSS probe over the P₉-P₂₀ area. A scheme of sample's P₉-P₁₇ area was positioned over the cross sectional profile to indicate the correspondence between CPD peaks and the different sample's layers. AFM detuning frequency was $\Delta f = -10$ Hz. FM KPFM was implemented using a modulation frequency $f = 1$ kHz and electrostatically excited with $V_{ac} = 500$ mV.

CONCLUSION

In this study, we proposed and demonstrated a protocol for KPFM probe's WF calibration, which was used for the acquisition of spatially resolved WF measurements. For this, we used non-contact AFM combined with single-pass FM-KPFM under UHV. We demonstrated why HOPG is not a well-suited reference sample for WF measurements. Instead, we proposed three different metallic samples with known crystallographic orientations as WF reference samples. Furthermore, we demonstrated the importance of UHV conditions when performing WF measurements, as measurements can vary largely due to absorbed water and other atmospheric contaminants on both the probe's and sample's surfaces. Furthermore, the implementation of non-contact AFM combined with FM-KPFM was considered necessary in order to avoid sample-probe physical contact which could lead to surface modifications, hence WF variation.

Sample preparation was proven of utmost importance for the probe's calibration precision. Using metallic reference samples we successfully calibrated a PtIr-PPP-EFM probe with an uncertainty of 0.03 eV. This calibrated probe was used to measure the absolute WF value on the HOPG ZYB grade sample, where we found $\phi = 4.6 \pm 0.03$ eV. Moreover, we also mapped the WF local variation over a nanostructured semiconductor sample presenting Al_{0.7}Ga_{0.3}As and GaAs layers with variable thickness. Finally, using the proposed protocol we calibrated a SSS probe which was used to investigate the local WF variation of the nanometer-thick layers on the same nanostructured sample. WF values found over this sample are in good agreement with the previously reported values over similar samples.⁶⁴

Summarizing, this approach allows the acquisition of absolute and reproducible WF values with an improved uncertainty with respect to often used HOPG-based protocols. Besides, the developed protocol allows the local investigation of the absolute WF value over nanostructured samples and can be applied for characterization of different electronic structures and devices.

ACKNOWLEDGMENTS

We acknowledge Denis Mariolle for helpful discussions. This work was supported by the French "Recherche Technologique de Base" program.

- ¹D. Cahen and A. Kahn, *Adv. Mater.* **15**, 271 (2003).
- ²A. Kahn, *Mater. Horiz.* **3**, 7 (2016).
- ³R. Schlaf, H. Murata, and Z. H. Kafafi, *J. Electron Spectrosc. Relat. Phenom.* **120**, 149 (2001).
- ⁴A. Mohamed and L. André, *J. Phys. D: Appl. Phys.* **31**, 1301 (1998).
- ⁵L. Kelvin, *London, Edinburgh, Dublin Philos. Mag. J. Sci.* **46**, 258 (1898).
- ⁶K. Siegbahn, C. Nordling, A. Fahlman, R. Nordberg, K. Hamrin, J. Hedman, G. Johansson, T. Bergmark, S.-E. Karlsson, I. Lindgren, and B. Lindberg, "ESCA: Atomic, molecular and solid state structure studied by means of electron spectroscopy," in *Nova Acta Regiae Societatis Scientiarum Upsaliensis*, Series IV, Volume 20 (North-Holland, 1967).
- ⁷J. Rabalais, *Principles of Ultraviolet Photoelectron Spectroscopy* (John Wiley and Sons, New York, 1977).
- ⁸M. Nonnenmacher, M. P. O'Boyle, and H. K. Wickramasinghe, *Appl. Phys. Lett.* **58**, 2921 (1991).
- ⁹M. Bohmisch, F. Burmeister, A. Rettenberger, J. Zimmermann, J. Boneberg, and P. Leiderer, *J. Phys. Chem. B* **101**, 10162 (1997).
- ¹⁰T. Glatzel, M. Rusu, S. Sadewasser, and M. C. Lux-Steiner, *Nanotechnology* **19**, 145705 (2008).
- ¹¹W. N. Hansen and G. J. Hansen, *Surf. Sci.* **481**, 172 (2001).
- ¹²A. Liscio, V. Palermo, K. Müllen, and P. Samorì, *J. Phys. Chem. C* **112**, 17368 (2008).
- ¹³C. Sommerhalter, T. W. Matthes, T. Glatzel, A. Jäger-Waldau, and M. C. Lux-Steiner, *Appl. Phys. Lett.* **75**, 286 (1999).
- ¹⁴C. H. Kim, C. D. Bae, K. H. Ryu, B. K. Lee, and H. J. Shin, *Solid State Phenom.* **124-126**, 607 (2007).
- ¹⁵C. Kim, B. Lee, H. J. Yang, H. M. Lee, J. G. Lee, and H. Shin, *J. Korean Phys. Soc.* **47**, 243 (2005).
- ¹⁶V. Palermo, M. Palma, Ž. Tomović, M. D. Watson, R. Friedlein, K. Müllen, and P. Samorì, *ChemPhysChem* **6**, 2371 (2005).
- ¹⁷H. Kawano, *Prog. Surf. Sci.* **83**, 215 (2008).
- ¹⁸P. G. Schroeder, M. W. Nelson, B. A. Parkinson, and R. Schlaf, *Surf. Sci.* **459**, 349 (2000).
- ¹⁹B. Reihl, J. K. Gimzewski, J. M. Nicholls, and E. Tosatti, *Phys. Rev. B* **33**, 5770 (1986).
- ²⁰S. J. Sque, R. Jones, and P. R. Briddon, *Phys. Status Solidi A* **204**, 3078 (2007).
- ²¹D. Martinez-Martin, R. Longinhos, J. G. Izquierdo, A. Marele, S. S. Alexandre, M. Jaafar, J. M. Gómez-Rodríguez, L. Bañares, J. M. Soler, and J. Gomez-Herrero, *Carbon* **61**, 33 (2013).
- ²²O. Ochedowski, B. K. Bussmann, B. B. d'Etat, H. Lebius, and M. Schleberger, *Appl. Phys. Lett.* **102**, 153103 (2013).
- ²³Y. Lu, M. Muñoz, C. S. Steplecaru, C. Hao, M. Bai, N. Garcia, K. Schindler, and P. Esquinazi, *Phys. Rev. Lett.* **97**, 076805 (2006).
- ²⁴S. Sadewasser and T. Glatzel, *Phys. Rev. Lett.* **98**, 269701 (2007).
- ²⁵W. Melitz, J. Shen, A. C. Kummel, and S. Lee, *Surf. Sci. Rep.* **66**, 1 (2011).
- ²⁶P. Bleuet, P. Cloetens, P. Gergaud, D. Mariolle, N. Chevalier, R. Tucoulou, J. Susini, and A. Chabli, *Rev. Sci. Instrum.* **80**, 069902 (2009).
- ²⁷S. Pouch, M. Amato, M. Bertocchi, S. Ossicini, N. Chevalier, T. Mélin, J.-M. Hartmann, O. Renault, V. Delaye, D. Mariolle, and L. Borowik, *J. Phys. Chem. C* **119**, 26776 (2015).
- ²⁸R. García and A. San Paulo, *Phys. Rev. B* **60**, 4961 (1999).
- ²⁹G. Li, B. Mao, F. Lan, and L. Liu, *Rev. Sci. Instrum.* **83**, 037101 (2012).
- ³⁰A. W. Dweydari and C. H. B. Mee, *Phys. Status Solidi A* **17**, 247 (1973).
- ³¹P. O. Gartland, *Phys. Norv.* **6**(3-4), 201 (1972).
- ³²R. M. Eastment and C. H. B. Mee, *J. Phys. F: Met. Phys.* **3**, 1738 (1973).
- ³³H. E. Farnsworth and R. P. Winch, *Phys. Rev.* **58**, 812 (1940).
- ³⁴K. Giesen, F. Hage, F. J. Himpsel, H. J. Riess, and W. Steinmann, *Phys. Rev. Lett.* **55**, 300 (1985).
- ³⁵S. Ryu, J. Chang, and S. K. Kim, *J. Chem. Phys.* **123**, 114710 (2005).
- ³⁶M. Chelvayohan and C. H. B. Mee, *J. Phys. C: Solid State Phys.* **15**, 2305 (1982).
- ³⁷K. Giesen, F. Hage, F. J. Himpsel, H. J. Riess, W. Steinmann, and N. V. Smith, *Phys. Rev. B* **35**, 975 (1987).
- ³⁸W. Y. Li, K. Goto, and R. Shimizu, *Surf. Interface Anal.* **37**, 244 (2005).
- ³⁹H.-N. Li, X.-X. Wang, S.-L. He, K. Ibrahim, H.-J. Qian, R. Su, J. Zhong, M. I. Abbas, and C.-H. Hong, *Surf. Sci.* **586**, 65 (2005).
- ⁴⁰D. Straub and F. J. Himpsel, *Phys. Rev. B* **33**, 2256 (1986).

- ⁴¹S. K. Kim, J. S. Kim, J. Y. Han, J. M. Seo, C. K. Lee, and S. C. Hong, *Surf. Sci.* **453**, 47 (2000).
- ⁴²G. A. Haas and R. E. Thomas, *J. Appl. Phys.* **48**, 86 (1977).
- ⁴³T. Wegehaupt, D. Rieger, and W. Steinmann, *Phys. Rev. B* **37**, 10086 (1988).
- ⁴⁴J. E. Rowe and N. V. Smith, *Phys. Rev. B* **10**, 3207 (1974).
- ⁴⁵G. G. Tibbetts, J. M. Burkstrand, and J. C. Tracy, *Phys. Rev. B* **15**, 3652 (1977).
- ⁴⁶T. A. Delchar, *Surf. Sci.* **27**, 11 (1971).
- ⁴⁷R. W. Strayer, W. Mackie, and L. W. Swanson, *Surf. Sci.* **34**, 225 (1973).
- ⁴⁸J. K. Grepstad, P. O. Gartland, and B. J. Slagsvold, *Surf. Sci.* **57**, 348 (1976).
- ⁴⁹A. J. Maxwell, P. A. Brühwiler, D. Arvanitis, J. Hasselström, M. K. J. Johansson, and N. Mårtensson, *Phys. Rev. B* **57**, 7312 (1998).
- ⁵⁰H. B. Michaelson, *J. Appl. Phys.* **48**, 4729 (1977).
- ⁵¹G. N. Derry, M. E. Kern, and E. H. Worth, *J. Vac. Sci. Technol., A* **33**, 060801 (2015).
- ⁵²J. C. Riviere, *Work Function: Measurements and Results* (Dekker, New York, 1969).
- ⁵³J. Hölzl and F. K. Schulte, "Work function of metals," in *Solid Surface Physics*, Springer Tracts in Modern Physics Vol. 85, edited by J. Hölzl, F. K. Schulte, and H. Wagner (Springer, Berlin, Heidelberg, 1979).
- ⁵⁴H. C. Potter and J. M. Blakely, *J. Vac. Sci. Technol.* **12**, 727 (1975).
- ⁵⁵C. Barth, T. Hynninen, M. Bielezki, C. R. Henry, A. S. Foster, F. Esch, and U. Heiz, *New J. Phys.* **12**, 093024 (2010).
- ⁵⁶E. Inami and Y. Sugimoto, *Phys. Rev. Lett.* **114**, 246102 (2015).
- ⁵⁷E. Taglauer, *Appl. Phys. A: Solids Surf.* **51**, 238 (1990).
- ⁵⁸Y. Almadori, Ł. Borowik, N. Chevalier, and J. C. Barbé, *Nanotechnology* **28**, 045306 (2017).
- ⁵⁹B. V. Andryushechkin, V. V. Cherkez, E. V. Gladchenko, G. M. Zhidomirov, B. Kierren, Y. Fagot-Revurat, D. Malterre, and K. N. Eltsov, *Phys. Rev. B* **84**, 075452 (2011).
- ⁶⁰C. P. A. Czanderna and T. Madey, *Specimen Handling, Preparation, and Treatments in Surface Characterization* (Kluwer Academic, New York, Boston, Dordrecht, London, Moscow, 1998).
- ⁶¹Y. Kuk, P. J. Silverman, and F. M. Chua, *J. Microsc.* **152**, 449 (1988).
- ⁶²E. Palacios-Lidón, C. R. Henry, and C. Barth, *ACS Catal.* **4**, 1838 (2014).
- ⁶³M. Senoner, T. Wirth, W. Unger, W. Österle, I. Kaiander, R. L. Sellin, and D. Bimberg, *Surf. Interface Anal.* **36**, 1423 (2004).
- ⁶⁴S. Pouch, F. Triozon, N. Chevalier, T. Melin, Y. M. Niquet, and Ł. Borowik, *RSC Adv.* **6**, 6782 (2016).
- ⁶⁵K. K. Ng and S. M. Sze, *Physics of Semiconductor Devices* (John Wiley & Sons, Inc., New York, 1981).
- ⁶⁶S. R. M. Levinshtein and M. Shur, *Handbook Series on Semiconductor Parameters* (World Scientific Publishing Co. Pte. Ltd., London, 1999).
- ⁶⁷S. Bastide, R. Butruille, D. Cahen, A. Dutta, J. Libman, A. Shanzer, L. Sun, and A. Vilan, *J. Phys. Chem. B* **101**, 2678 (1997).
- ⁶⁸M. Takashi, U. Takao, K. Shigeru, and M. Koichi, *Jpn. J. Appl. Phys., Part 2* **38**, L1321 (1999).